UNSTEADY RANS OF COMPLEX 3D TURBULENT FLOWS USING OVERSET GRIDS

Liang Ge, Joongcheol Paik, S Casey Jones, Fotis Sotiropoulos
School of Civil and Environmental Engineering
Georgia Institute of Technology
Atlanta, GA 30332-0355 USA

ABSTRACT

A numerical method is developed for solving the unsteady Reynolds-averaged Navier-Stokes (URANS) and turbulence closure equations in complex, multi-connected, 3D geometries. The governing equations are solved with a second-order-accurate finite-volume, dual-time-stepping artificial compressibility approach. Arbitrarily complex geometries are handled using domain decomposition with overset (Chimera) grids. The method is applied to simulate turbulent flows in two three-dimensional configurations inspired by the geometry of real-life bridge foundations in natural rivers: a channel with four bottom-mounted rectangular piers and a channel with a corner-mounted rectangular block. Comparisons between the computed results and laboratory measurements and flow visualization experiments lead to the conclusion that even relatively simple turbulence closure models (such as the standard k-ε model with wall functions or the one-equation Spalart-Allmaras model) can simulate flows with large-scale coherent structures with reasonable accuracy.

INTRODUCTION

Statistical turbulence models that directly resolve large-scale, organized, unsteady structures in the flow, such as unsteady RANS (URANS) or hybrid URANS/LES approaches, constitute the only feasible modeling framework for quantitatively accurate predictions of complex engineering flows at real-life Reynolds numbers (Spalart, 2000). Such strategies have already been applied with promising results in many complex engineering flow simulations. Hedges et al. (2002) used the detached-eddy simulation approach to study the flow around a generic airliner landing-gear truck. Yao et al. (2002) simulated turbulent trailing edge flows using a URANS approach.

The successful implementation and evaluation of unsteady, statistical turbulence modeling approaches in real-life engineering applications relies largely on the development of numerical methods capable of resolving arbitrarily complex geometrical configurations with high spatial and temporal resolution. In this paper we seek to: (1) develop an accurate numerical method for carrying out URANS computations in arbitrarily complex geometries; (2) illustrate the promise of the method in complex, 3D flows dominated by large-scale vortex shedding; and (3) assess the predictive capabilities of relatively simple isotropic turbulent models, including the standard k-ε model and the Spalart-Allmaras model (Spalart and Allmaras, 1994), in the context of URANS modeling.

We employed the domain-decomposition approach with structured, overset (Chimera) grids for discretizing complex, multi-connected geometries. The history of domain-decomposition can be tracked back to the pioneering, 19th century work by Schwartz (1869) who proposed an iterative method, known as Schwartz alternating procedure, to solve boundary value problems. The more recent implementation of this method in CFD was proposed by Steger et al. (1983). This method divides a complex domain into a number of simpler blocks or sub-domains. The sub-domains are allowed to arbitrarily overlap with each other and are discretized using structured, curvilinear grids. Such a grid arrangement is desirable because it exhibits much of the versatility of unstructured grids when handling complex geometries while retaining a number of desirable features of structured meshes. Grid components can be added or altered to represent the arbitrary shape of real-life geometries, thus permitting a great deal of flexibility in the discretization of multi-connected domains. Since each sub-domain is discretized using a structured grid, higher-order spatial discretization schemes and efficient temporal integration schemes can be easily implemented. It is also straightforward to selectively cluster the grid near solid surfaces without distorting the rest of the grid system, a feature which is highly desirable in turbulent flow simulations. Another attractive feature of the overlapping grids is that they provide a natural level of parallelism for execution on modern parallel computers. A major challenge in the implementation of overset grids in the context of URANS simulations, however, is the need for careful treatment of the flow variables at subdomain boundaries to ensure that vortical structures generated in one subdomain can cross grid interfaces and interact with the flow in adjacent subdomains without distortion (Tang et al., 2003).

In this work, we extend the overset-grid approach developed by Tang et al. (2003) to turbulent flows and apply it to carry out URANS simulations for two geometrical configurations inspired by real-life bridge foundations in natural rivers. The first test case is the flow past a bundle of wall-mounted rectangular piers. The specific geometry is shown

in Fig. 1 and is the actual foundation geometry of a bridge over the Chattahoochee River in southern Georgia, USA. The bundle consists of four rectangular piers located one behind the other along the flow direction. The geometry is further complicated by the rectangular concrete slab connecting the two middle piers, which, as shown in Fig. 1, does not extend all the way to the channel bed. The entire bridge foundation consists of four such bundles across the bridge span. The second example is a typical bridge abutment geometry consisting of rectangular block attached in the junction region between the side and bottom walls of a rectangular open channel as shown in Fig. 6. To illustrate the versatility of the overset grid approach we perform simulations with two different turbulence models. For the first case we employ the standard k-ε model with wall functions to bridge the gap between the logarithmic region and the laminar sublayer. For the second case, we employ the Spalart-Allmaras model in conjunction with a fine grid near the wall to directly resolve the flow in the laminar sublayer. The computed results are compared with mean velocity measurements and images from flow visualization experiments obtained in the Hydraulics Laboratory of the Georgia Institute of Technology.

In the following, we briefly describe the governing (URANS and turbulence closure) equations and the overset grid numerical method used in this work. We then discuss results from each of the examples in turn showing the complexity of each flow and presenting comparisons with available experiments.

GOVERNING EQUATIONS

The 3D, incompressible URANS equations formulated in generalized curvilinear coordinates read in compact tensor notation as follows:

$$\Gamma \frac{\partial Q}{\partial t} + J \frac{\partial}{\partial \xi^j} \left(F^j - F_v^j \right) = 0 \qquad (1)$$

where

$$\Gamma = \text{diag}\,[0\,1\,1\,1]$$

$$Q = [p, u_1, u_2, u_3]^T$$

$$F^j = \frac{1}{J} \left[U^j, u_1 U^j + p\xi^j_{x_1}, u_2 U^j + p\xi^j_{x_2}, u_3 U^j + p\xi^j_{x_3} \right]^T$$

$$F_v^j = \frac{1}{J} \left(\frac{1}{Re} + \nu_t \right) \left[0, g^{mj} \frac{\partial u_1}{\partial \xi^m}, g^{mj} \frac{\partial u_2}{\partial \xi^m}, g^{mj} \frac{\partial u_3}{\partial \xi^m} \right]^T$$

In the equations above, p is the static pressure divided by the density, u_i $(i = 1,2,3)$ are the mean Cartesian velocity components, x_i are the Cartesian coordinates, J is the Jacobian of the geometric transformation, ν_t is the eddy viscosity that is calculated from the turbulence model, $\xi^j_{x_i}$ are the metrics of the geometric transformation, U^j are the contravariant velocity components, g^{ij} are the components of the contravariant metric tensor, and Re is the Reynolds number.

For the bridge pier configuration, we use the standard k-ε turbulence model with wall functions for turbulence closure. The model equations are used in their well-known standard form and are not included here due to space limitations. To simulate bed roughness in this geometry, we employ the following generalized wall functions:

$$u^+ = \frac{1}{\kappa} \left[\ln \left(y^+ \right) \right] + B - \Delta B \qquad (2)$$

with $u^+ = u/U_\tau$ and $y^+ = U_\tau y/\nu$ where U_τ is the friction velocity. The velocity shift ΔB for uniform sand-grain roughness is a a function of the bed roughness height $k_s^+ = U_\tau k_s/\nu$. In this study, we used the velocity shift formulation of Cebeci and Bradshaw (1977) which reads as

$$\Delta B = \left[B - 8.5 + \frac{1}{\kappa} \ln \left(k_s^+ \right) \right] \sin \left[0.4258 \left(\ln \left(k_s^+ \right) - 0.811 \right) \right]$$

$$\text{for } 2.25 \le k_s^+ \le 90 \text{ and}$$

$$\Delta B = B - 8.5 + \frac{1}{\kappa} \ln \left(k_s^+ \right) \quad \text{for } k_s^+ \ge 90$$

The wall functions are implemented using the two-point approach described in detail in Sinha et al. (1998). For the bridge-abutment simulation we employ the Spalart-Allmaras turbulence model in its standard form.

NUMERICAL METHOD AND OVERLAPPING DOMAIN-DECOMPOSITION APPROACH

The governing equations are discretized in space using a three-point central-difference, second-order-accurate, finite-volume scheme. Third-order, fourth-difference, matrix-valued artificial dissipation terms (Lin and Sotiropoulos, 1997) are explicitly added to the discrete equations to suppress grid-scale oscillations. The discrete equations are integrated in time using a second-order-accurate, dual-time-stepping, artificial compressibility scheme. We integrated the equations in pseudo time using the Beam-and-Warming approximate-factorization scheme. Typically 20 pseudo iterations were required to reduce all residuals by three orders of magnitude.

We illustrate our overlapping domain-decomposition method for the geometrically more complicated bridge pier example. As shown in Fig. 1, a background Cartesian grid is used to discretize the *empty* rectangular open channel and three O-type grids, tailored to resolve the geometrical features of the piers, are embedded within the background grid. The fact the rectangular slab connecting the two middle piers does not extend all the way to the bottom is accounted for by embedding a rectangular sub-domain just for this slab. Such an approach leads to a set of five structured sub-domains. On each sub-domain, an individual set of governing equations are solved. A converged solution to the original flow problem is obtained by iterating on each sub-domain and communicating boundary conditions at each boundary interface to the connecting domain via interpolation.

The interface interpolation is implemented in two steps. First we determine the location of each grid node on the interface relative to the other domains using a Newton method. Tang (2001) gives a detailed description of the grid-connectivity procedure. This grid connectivity information can be performed as a preprocessing step and stored for use during the calculation. The second step is the interpolation of the flow variables from the background domain to the interface of interest. Since we employ a second-order spatial-discretization scheme for our flow solver, a second-order interpolation scheme is required to maintain the overall accuracy. The code we have developed features both standard trilinear interpolation for all flow variables at grid interfaces (Steger et al., 1983) as well as the so-called mass-flux based interpolation approach developed in Tang et al. (2003). This latter interpolation algorithm is based on enforcing a second-order accurate discrete approximation of

global mass conservation at each overset grid interface and has been shown to enhance the overall efficiency of the numerical algorithm as well as the smoothness of the computed solution across interfaces as compared to the standard trilinear approach, especially when the grid spacing of adjacent subdomains is discontinuous.

Note that in the work of Tang et al. (2003) the governing equations were solved using an explicit (Runge-Kutta) dual-time-stepping artificial compressibility iteration scheme. Tang et al. (2003) were able to obtain good results with this approach for a number of complex laminar flows, but our early attempts to extend their explicit iterative scheme to URANS simulations were not successful. Extensive numerical tests showed that when applying this method to solve the URANS and turbulence closure equations, numerical instabilities develop at grid interfaces during the early stages of the dual-time-stepping iteration scheme. These instabilities were linked to the production terms in the turbulence closure equations, which depend on products of velocity gradients. Such terms impose more stringent smoothness requirements than in laminar flow simulations because both the velocity field and its gradients across grid interfaces should be smooth. In fact we found that to avoid numerical instabilities during the early stages of the simulation, a smooth velocity field across interfaces needs to be established within as few dual-time-stepping iterations as possible. The more robust approximate factorization method we employ in this work was found sufficient to alleviate this problem and to allow efficient and stable unsteady simulations over long time intervals.

FLOW PAST A BUNDLE OF WALL-MOUNTED RECTANGULAR PIERS

In this section, we apply our URANS method with the standard k-ε model to simulate the flow around a complex bridge pier geometry based on an actual foundation of a Chattahoochee River bridge (Georgia, USA). The actual foundation has four sets of piers that span the river. In this study, we simulate the flow around only one set as shown in Fig. 1. The computational domain is a $40\,\mathrm{b} \times 7\,\mathrm{b}$ rectangular domain, where b is the width of the first bridge pier (Pier 1 in Fig. 1). The water depth is $\mathrm{d} = 3.2\,\mathrm{b}$ and the river bed is assumed to be flat. The computational grid contains 5 blocks giving an approximate total of 1 million active grid nodes. Calculations were carried out for $Re = 100,000$ based on the water depth and the bulk velocity at the inlet of the domain. The non-dimensional physical time step was $\Delta t = 0.25$. At the inlet, we specified fully developed turbulent flow. The free-surface was treated as a flat rigid lid and extrapolation was used to specify boundary conditions for all flow variables at the outflow and lateral boundaries of the computational domain. The URANS simulation was conducted for 5000 time steps to obtain a statistically converged mean flow field. Measurements of the flow around this foundation geometry were conducted in the Hydraulics laboratory at Georgia Tech using a 1:20 scale model. Model runs were conducted in flat-bed flume, and the bed was composed of sand with $d_{50} = 3.3\,\mathrm{mm}$ (hydraulically fully rough regime). Mean velocity measurements were obtained using an acoustic Doppler velocimeter (ADV).

Figure 2 shows instantaneous and time-average axial velocity contours on a horizontal plane just below the surface. The two snapshots (Fig.2a,b) demonstrate the complex nature of the flow and show the large-scale instabilities of the shear layers emanating from the solid walls, which lead to asymmetric vortex shedding. It is important to note that large-scale unsteadiness and asymmetry develop naturally in our simulations, as the governing equations are iterated in time, without imposing any kind of explicit forcing on the approach flow. Also note that the vortices generated by the multiple piers are transported downstream, crossing boundaries of various overset grids smoothly without spurious distortions. Figure 2c shows the time-average velocity field obtained by averaging the solution over the entire simulated interval (5000 time steps). As anticipated, the time-average flow is symmetric about the horizontal centerline and is characterized by shear-layers emanating from each pier and zones of reverse flow in the pier wakes.

The three-dimensional complexity of the instantaneous flow is shown in Fig. 3, which shows a snapshot of instantaneous particle paths around the piers. The instantaneous flow field is composed of an intricate web of horseshoe- and tornado-like vortices. Video animations show that these large-scale vortices appear and disappear periodically throughout the entire simulated time interval.

To validate our computations, we compare the simulated time-average streamwise velocity field with the experimental results. The comparisons are shown in Fig. 4, which depict time-average streamwise velocity profiles at six different planes that are perpendicular to the flow direction. The locations are shown in Fig. 1: planes F1 and F2 are located at $0.5\,\mathrm{d}$ and $0.2\,\mathrm{d}$, respectively, upstream of the first bridge pier; plane F3 is the vertical plane of symmetry of the first pier; plane F4 lies halfway between the last two bridge piers; and planes F5 and F6 are downstream of the last bridge pier. On every plane, we compare the velocity profiles at three depths: $0.2\,\mathrm{d}$, $0.4\,\mathrm{d}$, and $0.6\,\mathrm{d}$ measured from the bottom. As shown in these figures, our calculations capture all experimental trends with good accuracy. This level of agreement between the computations and the measurements is encouraging given the enormous complexity of the flow and the fact that the standard k-ε model was used for turbulence closure.

The agreement between our computations and the measurements is especially good in the wake of the four piers. This trend should be attributed to the fact that in this region the flow is dominated by the interactions of the upstream shed large-scale unsteady vortices, which are directly resolved in our simulation. Fig. 5 compares contours of resolved and modeled (time average k predicted by the k-ε model) turbulence kinetic energy at one horizontal plane. As shown in the figure, the large-scale structures in the flow are responsible for producing most of the total turbulence kinetic energy in the wake region while the turbulence model accounts for most of the kinetic energy upstream of the last pier.

FLOW PAST A CORNER-MOUNTED RECTANGULAR BLOCK

The geometry of the second test case consists of a rectangular block mounted in the junction region between the bottom and side walls of a rectangular open channel with a flat bed. The Re of 100,000 is based on the mean approach velocity and the length of the block L. The ratio of flow depth to the abutment length is $L/d = 5$. Two overset grids are used to discretize this geometry as shown in Fig. 6: a Cartesian background grid for the channel and a curvilinear, O-type grid for the region around the obstacle. The total number of active grid nodes in this overset grid layout is 900,000. The non-dimensional physical time

step was $\Delta t = 0.025$. As mentioned above, we used the one-equation Spalart-Allmaras model to close the URANS equations. Flow visualization experiments for this geometry have been reported by Chrisohoides and Sotiropoulos (2003) who developed a novel experimental technique for visualizing and extracting the time scales of coherent vortices at the free surface.

The general features of this flow as derived by our simulations and recent visualization experiments (Chrisohoides et al. (2003), Chrisohoides and Sotiropoulos (2003)) can be summarized as follows. As the upstream flow approaches the obstacle, it encounters a strong transverse pressure gradient that diverts it around the obstacle. A large region of recirculating flow forms at the upstream junction between the obstacle and the channel side wall. The flow within this upstream recirculating region is very complex consisting of multiple, large-scale eddies, which appear and disappear in a seemingly random manner. A slowly evolving, large recirculating zone is also present at the downstream end of the obstacle, and a shear layer develops at the interface between the slow moving fluid within this zone and the flow diverted around the obstacle. These complex features are illustrated in Fig. 7, which shows an instantaneous snapshot of the ω_z vorticity contours at the surface. The interface of the O-type overset grid is also included in the figure to further underscore the ability of our domain decomposition approach to allow for complex vortical structures to cross undisturbed from one subdomain to another.

As discussed above, Chrisohoides et al. (2003) showed that the flow in the upstream recirculation zone consists of multiple, large-scale eddies with very rich dynamics. The number and structure of these eddies varies continuously in time. There are instants in time when a single eddy occupies the center of the upstream recirculating zone. This eddy was shown to split into two eddies, which are rotated by the flow in the counter-clockwise direction, merge to form a larger eddy, and subsequently could bifurcate again to form two or more eddies. These complex processes were found to emerge repeatedly in a random manner. Chrisohoides et al. (2003) also showed that the upstream corner of the upstream recirculating zone exhibits similar rich dynamics with multiple smaller-scale eddies appearing and disappearing randomly. Video animations of calculated instantaneous streamlines show that our numerical solutions exhibit very similar patterns as those observed in the laboratory. Representative snapshots of the visualized and simulated instantaneous coherent eddies in the upstream recirculating region are shown in figures 8 and 9. As shown in these figures, the calculated streamlines exhibit patterns that are in good agreement with the experimental images. Similar conclusions can be drawn from Fig. 10, which compares calculated instantaneous, snapshots of large-scale vortex shedding from the obstacle shear layer with the visualization images of Chrisohoides et al. (2003).

A rather remarkable feature of this flow is that it is characterized by regions of disparate time scales, such as the slowly evolving upstream and downstream recirculating regions and the unstable shear layer, which is dominated by high-frequency vortex shedding. The disparity of time scales and the richness of the temporal dynamics are illustrated in Fig. 11, which shows calculated time histories of the streamwise velocity at two points (locations are indicated in Figs. 8 and 10). Point a is located in the upstream recirculating region and point b is located within the shear layer. These two time histories underscore the ability of our method to simulate flows with very rich temporal large-scale dynamics.

CONCLUSIONS

We presented an overset grid URANS method for predicting turbulent flows in complex, multi-connected geometries. The method was applied to study two flow cases whose geometry was inspired by real-life bridge foundations using both wall functions and a turbulence closure model that is valid all the way to wall. Comparisons with flow visualization experiments show that the method captures many of the complex instantaneous, large-scale flow features observed in the laboratory. Quantitative comparisons with experimental measurements in terms of mean velocity profiles further underscore the ability of the URANS approach to predict complex flows with reasonable accuracy. Our work shows that (1) overset grids provide a powerful modeling framework for simulating complex, unsteady flows in multi-connected geometries; and (2) URANS with relatively simple turbulence closure models can be promising for quantitatively accurate predictions of very complex flows that are dominated by large-scale unsteadiness. Our future work will focus on more comprehensive quantitative validations of our method, assessment of the relative performance of various turbulence closure models, and investigation of the role of near-wall modeling versus wall functions in the context of the URANS approach.

ACKNOWLEDGMENTS

This work was supported by NSF Career grant 9875691, a grant from Georgia Department of Transportation, and a grant from Oak Ridge National Laboratory and DOE. We thank Terry W. Sturm for providing the experimental data for the first test case.

REFERENCES

T. Cebeci and P. Bradshaw. *Momentum Transfer in Boundary Layers*. Hemisphere, 1977.

A. Chrisohoides and F. Sotiropoulos. An experimental technique for visualizing lagrangian coherent structures in aperoidic flows. *Phys. of Fluids*, 15(3):25–28, 2003.

A. Chrisohoides, F. Sotiropoulos, and T. Sturm. Coherent structures in flat-bed abutment flows: Experiments and cfd simulations. *J. Hydr. Eng.*, 129(3):177–186, 2003.

L.S. Hedges, A. K. Travin, and P. R. Spalart. Detached-eddy simulations over a simplified landing gear. *J. of Fluids Eng.*, 124(2):413–423, 2002.

F. B. Lin and Fotis Sotiropoulos. Assessment of artificial dissipation models for three-dimensional incompressible flow solutions. *J. Fluids Eng.*, 119(2):331–340, 1997.

H. A. Schwartz. Uber einige abbildungsaufgaben. *Ges. Abh.*, 1869.

S. K. Sinha, F. Sotiropoulos, and A. J. Odgaard. Three-dimensional numerical model for flow through natural rivers. *J. of Hydr. Eng.*, 124(1):13–24, 1998.

P. R. Spalart. Strategies for turbulence modelling and simulations. *Int. J. of Heat and Fluid Flow*, 21:252–263, 2000.

P. R. Spalart and S. R. Allmaras. A one-equation turbulence model for aerodynamic flows. *La Recherche Aerospatiale*, 1:5–21, 1994.

J. Steger, F. C. Dougherty, and J. Benek. A chimera grid scheme; advances in grid generation. *ASME FED*, 5:59–69, 1983.

H. S. Tang. *Domain Decomposition Algorithms for 3D Unsteady Incompressible Flows.* PhD thesis, Georgia Institute of Technology, 2001.

H. S. Tang, S. Casey Jones, and Fotis Sotiropoulos. Domain decomposition with overset grids for 3D incompressible flows. submitted to the J. Comp. Phys., 2003.

Y. F. Yao, A. M. Savill, N. D. Sandham, and W. N. Dawes. Simulation and modelling of turbulent trailing-dege flow. *Flows Turb. and Comb.*, 68(4):313–333, 2002.

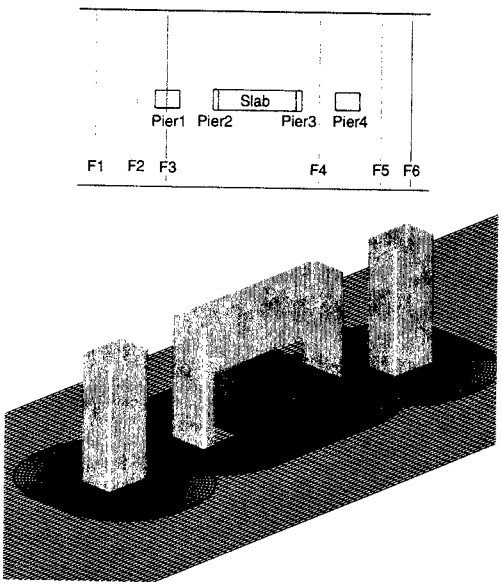

Figure 1: Geometry of bridge piers and overlapping grids.

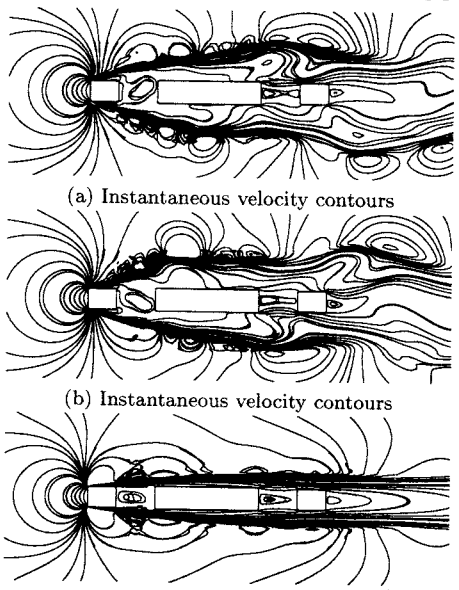

(a) Instantaneous velocity contours

(b) Instantaneous velocity contours

(c) Time average velocity contours

Figure 2: Streamwise velocity contours at a horizontal plane.

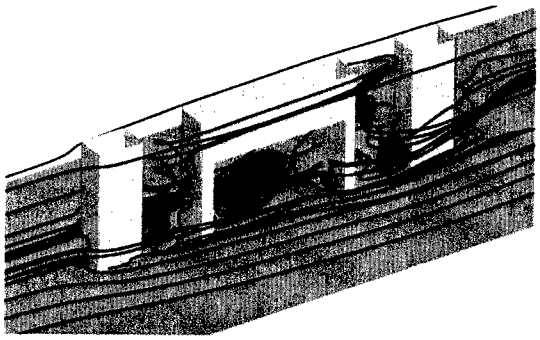

Figure 3: Instantaneous three-dimensional streamtraces depicting large-scale vortical structures.

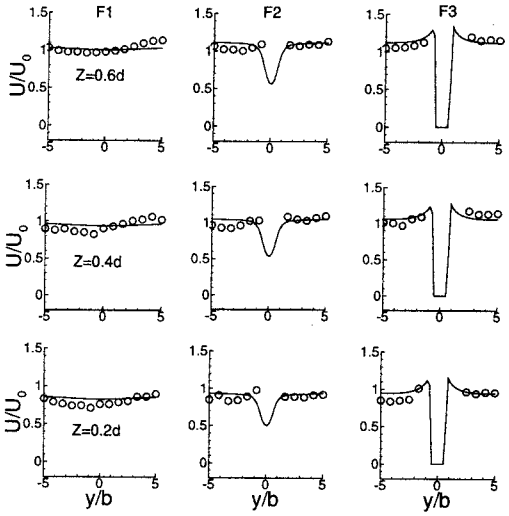

(a) Planes F1-F3

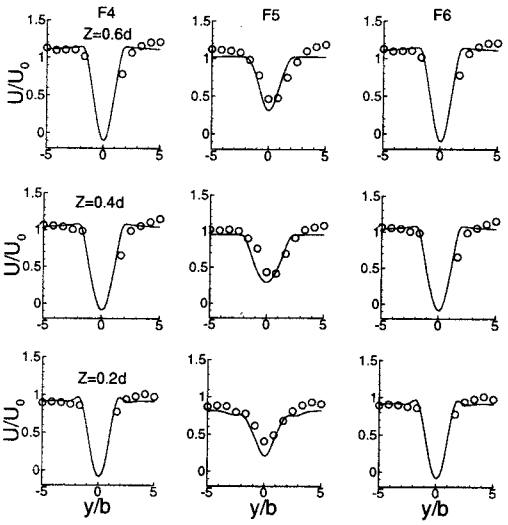

(b) Planes F4-F6

Figure 4: Streamwise mean velocity profile across the spanwise direction (—— simulation o experiment) (see Fig. 1 for plane locations).

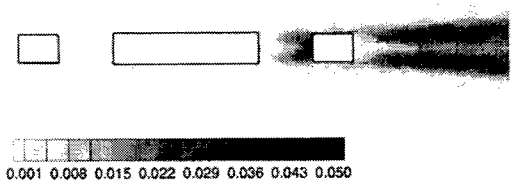

(a) Resolved by URANS simulation

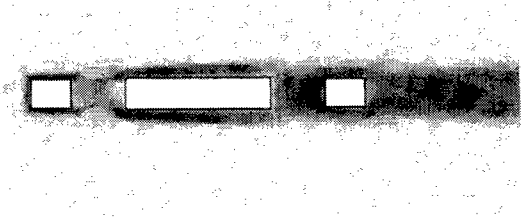

(b) Modeled by k-ε model

Figure 5: Contours of turbulence kinetic energy.

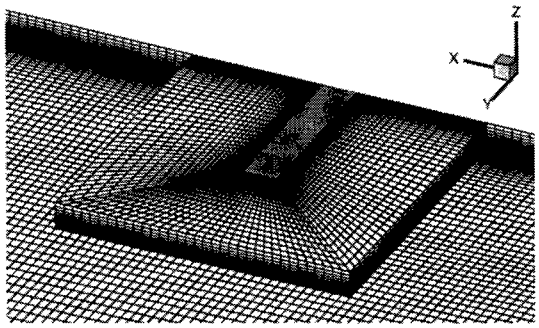

Figure 6: Geometry of the corner-mounted rectangular block and grid system.

Figure 7: Instantaneous vorticity contours at the free-surface

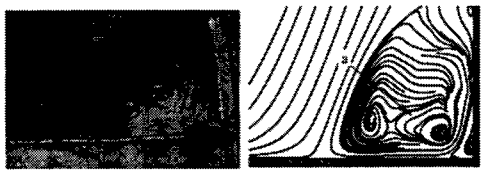

Figure 8: Visualized (Chrisohoides and Sotiropoulos, 2003) and predicted instantaneous streamlines near the junction of the obstacle wall with the side of the channel.

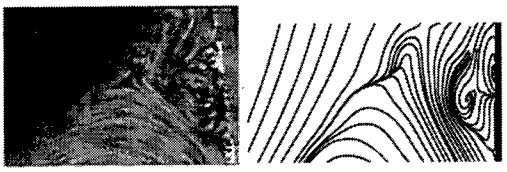

Figure 9: Visualized (Chrisohoides and Sotiropoulos, 2003) and predicted instantaneous streamlines near the upstream corner of the separation region.

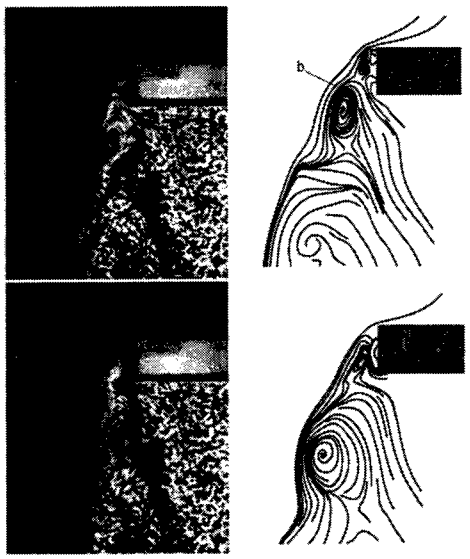

Figure 10: Time sequence of visualized (Chrisohoides et al., 2003) and predicted instantaneous streamlines in the shear layer.

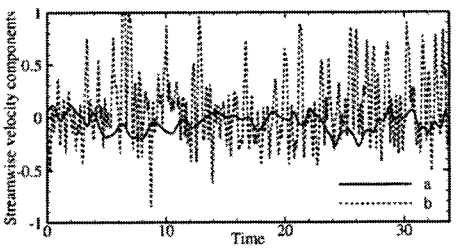

Figure 11: Time series of computed streamwise velocity components at two selected locations (see Fig. 8 and 10 for point locations).